ACS APPLIED MATERIALS & INTERFACES

Research Article

www.acsami.org

Photoelectrochemical Cells Utilizing Tunable Corroles

Bradley J. Brennan, Yick Chong Lam, Paul M. Kim, Xing Zhang, and Gary W. Brudvig*

Energy Sciences Institute and Department of Chemistry, Yale University, P.O. Box 208107, New Haven, Connecticut 06520-8107, United States

Supporting Information

ABSTRACT: Organic dyes with their wide range of molecular structures and spectroscopic features show great promise for solar energy applications. Corroles, structural analogues to porphyrins, are highly fluorescent molecules with tunable properties. We have synthesized a series of structurally similar corroles chelating gallium and phosphorus, along with a β-chlorinated phosphorus corrole, and determined their photophysical and electrochemical properties. The electrochemical potentials to oxidize the corroles range from 0.78 V vs NHE for the gallium corrole to 1.42 V for the β-octachlorinated phosphorus corrole. We are interested in developing photosensitizers for water oxidation on a metal oxide-based photoanode, so the corroles were modified to contain a *meso*-phenyl-COOH substituent for binding to metal oxide surfaces. The ability of these corrole dyes to act as photosensitizers was assessed by comparing the corroles in a model dye sensitized solar cell design. Transient absorption spectroscopy was utilized to analyze recombination dynamics and determine the kinetics of iodide oxidation. The most efficient photoelectrochemical cell was achieved for the phosphorus corrole P-2 with electrochemical properties and kinetics suitable for both photoinduced electron injection into TiO_2 and oxidation of iodide. This structure–function study highlights the wide window for tuning corrole electrochemical potentials while still maintaining desirable photophysical properties, important variables when designing dyes for applications in photoelectrochemical water-oxidation cells.

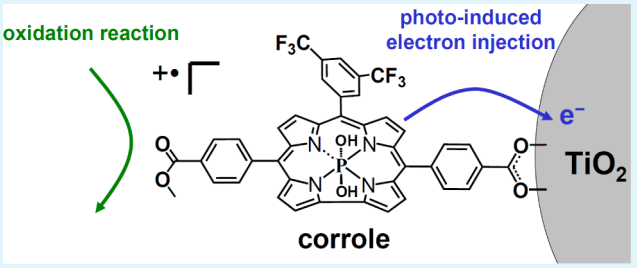

KEYWORDS: *corroles, molecular design, photoelectrochemical cells, nanosecond transient absorption spectroscopy, electrochemistry*

INTRODUCTION

Organic dyes are commonly used to photosensitize wide-bandgap metal oxides for photoelectrochemical cells such as photoelectrosynthetic designs and dye-sensitized solar cells (DSSC).[1−3] Porphyrin dyes are the current leaders in organic DSSC solar conversion efficiency, and trends in dye design are leading to ongoing improvements.[4] Porphyrins have also been utilized in photoelectrochemical water-oxidation designs, where the dye works in concert with a catalyst to convert H_2O into O_2 and H^+.[5] Corroles, synthetic analogues to porphyrins, have not been extensively examined for use in photoelectrochemical cells.[6,7] The most efficient photoelectrochemical cell to date, utilizing a tris-*meso*-pentafluorophenyl gallium corrole prepared by Walker and co-workers, had 1.6% solar conversion efficiency.[7] Previously, corroles with β-substituted linkers were used for attachment to metal oxides. Here, we compare the electrochemical and photophysical properties of model corrole structures containing *meso*-phenyl-COOH substituents, analyze their function in photoelectrochemical cells, and correlate their performance with their ability to photoinject an electron and the capability of the resulting dye radical cation species to oxidize a redox-active charge transport molecule in solution. By using these structure–function data to engineer a structurally simple dye capable of thermodynamically performing both tasks, we fabricated a photoelectrochemical cell with 1.9% solar conversion efficiency. The results demonstrate the use of chelated *p*-block elements and β-chlorination of corroles for modulating dye properties, and provide structure–function relationships for photoelectrochemical cell applications.

EXPERIMENTAL SECTION

Materials. 3,5-Bis(trifluoromethyl)benzaldehyde was obtained from Santa Cruz Biotech. Tetrachloro-*p*-benzoquinone and iodine were obtained from Acros Organics. *Tert*-butylpyridine (TBP) was obtained from Sigma-Aldrich. Lithium iodide, sodium perchlorate, tetrachloro-bis(tetrahydrofuran) titanium(IV), and hydrazine monohydrate were obtained from Alfa Aesar. Tetra-*n*-butylammonium hexafluorophosphate ($TBAPF_6$) was recrystallized from ethanol and dried. Transparent TiO_2 paste was obtained from Solaronix (Ti-Nanoxide T/SP) and opaque TiO_2 paste was obtained from Dyesol (18NR-AO). FTO-coated glass (TEC 15, 2.2 mm) was obtained from Hartford Glass.

Synthesis. Butylmethylimidazolium iodide and 5-(4-carbomethoxyphenyl)dipyrromethane have been prepared previously.[8,9] The corroles 10-(3,5-bis-trifluoromethylphenyl)-5,15-(methyl-4-carboxyphenyl) corrolato gallium(pyridyl) (Ga-1), 10-(3,5-bis-trifluoromethylphenyl)-5,15-(methyl-4-carboxyphenyl) corrolato phosphorus(dihydroxyl) (P-1), and 10-(3,5-bis-trifluoromethylphenyl)-5,15-(methyl-4-carboxyphenyl)-2,3,7,8,12,13,17,18-octachloro corrolato phosphorus(dihydroxyl) (PCl_8-1) were prepared from the metal-free derivative.[10] The monocarboxylic acid derivatives Ga-2, P-2, and PCl_8-2 were prepared via alkaline hydrolysis of the corresponding

Received: June 8, 2015
Accepted: July 2, 2015
Published: July 2, 2015

ACS Publications © 2015 American Chemical Society

DOI: 10.1021/acsami.5b05050
ACS Appl. Mater. Interfaces 2015, 7, 16124−16130

Ga-1, P-1, PCl_8-1 esters. Synthetic procedures and characterization details are described in the Supporting Information.

Methods. Proton NMR spectra were collected on a 400 MHz instrument in $CDCl_3$ or in $CDCl_3$ containing CD_3OD with an internal TMS standard. Coupling values (J) are reported in Hz and chemical shifts are reported as δ ppm from TMS. Mass spectrometry was performed with an Agilent Voyager DE Pro MALDI-TOF mass spectrometer. UV−visible spectroscopy was performed using a Shimadzu 2600. Steady-state and time-correlated single photon counting (TCSPC) spectrofluorimetry were performed in dichloromethane solvent using a Horiba FluoroLog (FL3-21) instrument with a Fluorohub TCSPC accessory and a TBX-04 detector. Uncorrected steady-state spectra were obtained by illuminating at 459 nm (Ga-1) or 390 nm (P-1, PCl_8-1). TCSPC was performed using a 566 nm (Ga-1) or 390 nm (P-1, PCl_8-1) nanoLED pulsed excitation with a 1.5 ns (566 nm) or 1.3 ns (390 nm) instrument response time. Fitting of the data was performed with the DAS6 software provided by Horiba. For Ga-1, 2% pyridine was added to maintain the axial ligand. Electrochemistry was performed with a Pine WaveNow-XV potentiostat. All data are referenced to the normal hydrogen electrode (NHE) using the ferrocene redox couple (0.72 V vs NHE) as an internal reference.[11] Working and counter electrodes were platinum, with a pseudo Ag/AgCl reference. The electrolyte consisted of 100 mM tetra-*n*-butylammonium hexafluorophosphate in dichloromethane. Spectroelectrochemistry was performed using a Shimadzu 2600+ integrating sphere, with bulk electrolysis to form the corrole radical cation species performed at ∼0.94, 1.43, or 1.73 V vs NHE for Ga-1, P-1, and PCl_8-1, respectively. For all experiments characterizing Ga-1, 2% pyridine was added to maintain the axial ligand.

Preparation of Electrodes. DSSCs were fabricated using a previously published method.[12] FTO-coated glass was cleaned with alkali detergent, water, and ethanol. A compact layer of TiO_2 was formed on the substrates by heating in a 40 mM aqueous solution of $TiCl_4$·2THF at 80 °C for 30 min; then the samples were rinsed with water and ethanol, and dried. The substrates were annealed in air by ramping 600 °C/h to 375 °C, holding for 5 min, ramping 300 °C/h to 570 °C, holding for 10 min, and slowly cooling. Transparent nanoparticulate TiO_2 films were produced by spreading TiO_2 paste (Solaronix) on the substrates with a mask consisting of Scotch Magic Tape, heating at 80 °C for 9 min, and repeating for a total of two layers. An additional opaque layer of TiO_2 was applied by the same method using highly scattering TiO_2 paste (Dyesol). The substrates were then annealed in air by ramping 180 °C/h to 370 °C for 10 min, ramping 180 °C/h to 470 °C for 30 min, and then slowly cooling. The substrates were then placed again in a 40 mM aqueous solution of $TiCl_4$·2THF using the procedure as discussed before. While the substrate electrodes were still warm, they were placed in a 0.15 mM solution of corrole in ethyl acetate. The electrodes were soaked overnight, rinsed in ethyl acetate, and dried under N_2 flow. Counter electrodes were prepared from FTO-coated glass containing a 2 mm hole. The counter electrode was platinized by placing a drop of 4% (w/w) H_2PtCl_6 and heating at 450 °C for 30 min. DSSCs were prepared by sandwiching the dye-sensitized electrode and counter electrode with 25 μm thermoplastic spacer (Surlyn, Solaronix), and sealed at 115 °C for 45 s. Electrolyte was introduced into the cell and the hole sealed using Surlyn.

Solar Characterization. Incident photon to current efficiency (IPCE) was obtained by illumination using monochromatic light from a xenon lamp and a single-grating monochromator. Power density was determined using a calibrated silicon diode (Newport 818-UV). Current−voltage (I−V) data were obtained under simulated sunlight by filtering a xenon lamp with an AM1.5G filter (Newport Corp) at 1000 W/m^2, with power density determined using a calibrated silicon diode (ASTM E948-09/ASTM E1021-06). IPCE and I−V data were obtained using a Keithley 2400 sourcemeter and LabView software.

Transient Absorption Spectroscopy. Sensitized TiO_2 electrodes were covered with either inert electrolyte (100 mM $LiClO_4$ and 100 mM *tert*-butylpyridine in acetonitrile solvent) or the DSSC electrolyte containing iodide (100 mM LiI, 50 mM I_2, 100 mM *tert*-butylpyridine, and 800 mM *n*-butylmethylimidazolium iodide in acetonitrile solvent), and then sandwiched with a microscope slide to prevent evaporation. The samples were placed in a 1 cm × 1 cm cuvette at a 45° angle relative to both the pump and probe beams. Time-resolved absorption measurements were carried out using a LP920 laser flash photolysis spectrometer (Edinburgh Instruments). The third harmonic of a Nd:YAG laser (Spectra-Physics Quanta-Ran INDI 40−10, operated at 1 Hz) was used to pump an optical parametric oscillator (OPO, Spectra-Physics, basiScan-M), which provided excitation in the visible region (3−5 ns pulses, ∼1 cm beam diameter, <300 μJ/pulse). White probe light was supplied by a pulsed 450 W Xe arc lamp. A combination of short- and long-pass filters was employed to remove stray light. Transmitted light was detected by a photomultiplier tube (PMT, Hamamatsu R928). The PMT current was amplified and recorded using a transient digitizer (Tektronix TDS 3032C).

RESULTS

The corrole dyes shown in Figure 1 were synthesized from the metal-free derivative prepared using the procedure of Koszarna

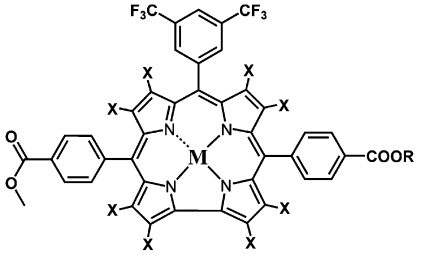

	M	X	R
Ga-1	Ga(pyr)	H	CH_3
Ga-2	Ga(pyr)	H	H
P-1	$P(OH)_2$	H	CH_3
P-2	$P(OH)_2$	H	H
PCl_8-1	$P(OH)_2$	Cl	CH_3
PCl_8-2	$P(OH)_2$	Cl	H

Figure 1. Synthesized corrole dyes. Gallium corroles coordinate an axial pyridine ligand (pyr) whereas the phosphorus corroles maintain two hydroxide (OH) axial ligands.

and co-workers.[10] The trivalent ligand stabilizes Ga^{3+} with an associated pyridyl ligand, and P^{5+} with two axial hydroxide ligands. Chlorination of the phosphorus corrole P-1 was performed using *N*-chlorosuccinimide, yielding PCl_8-1 with complete replacement of the eight β-H positions with Cl. The UV−visible absorbance spectra of the compounds in Figure 2 show typical features for gallium and phosphorus corroles.[13,14] The prominent Soret band (400−450 nm) and more weakly absorbing Q-bands (500−650 nm) are similar to those of metalloporphyrins.[15] The chlorinated derivative PCl_8-1 has a 7 nm bathochromic shift of the Soret band and 3 nm bathochromic shift of the Q-band near 600 nm compared to the nonchlorinated analogue. Fluorescence spectra shown in Figure S1 in the Supporting Information directly correlate with the absorbance features and trends for the corroles, with minimal Stokes shifts of ∼5 nm. Fluorescence lifetimes were obtained as single-exponential decays for Ga-1 (2.3 ns), P-1 (3.0 ns), and PCl_8-1 (660 ps), with spectra shown in Figure S2 of the Supporting Information. Electrochemistry provided electrochemical reduction potentials for the radical cation species generated by oxidation of the corroles (Figure 3). The first oxidation for each corrole was a reversible single electron process, but these potentials were significantly shifted among the dyes. Ga-1 was the easiest to oxidize at 0.78 V vs NHE, followed by P-1 at 1.08 V, and PCl_8-1 at 1.42 V. This equates to

DOI: 10.1021/acsami.5b05050
ACS Appl. Mater. Interfaces 2015, 7, 16124−16130

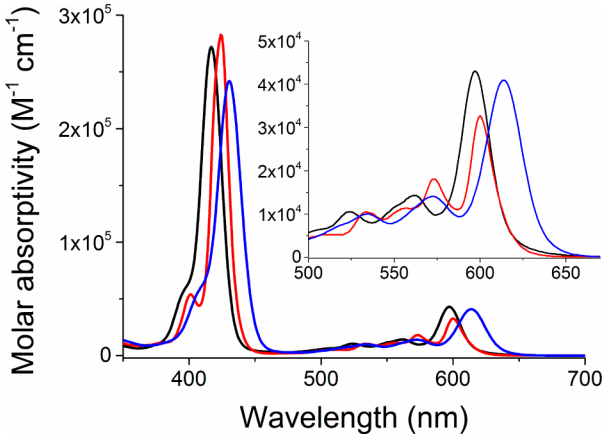

Figure 2. Corrole UV−visible absorbance spectra for Ga-1 (blue), P-1 (black), and PCl_8-1 (red). Inset highlights Q-band region. Experiment performed in dichloromethane. For Ga-1, 2% pyridine was added to maintain the axial ligand.

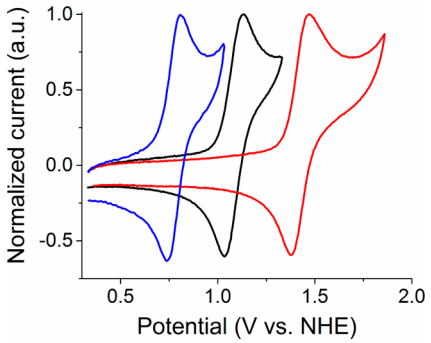

Figure 3. Corrole electrochemistry for Ga-1 (blue), P-1 (black), and PCl_8-1 (red). Cyclic voltammetry experiments performed in dichloromethane containing 100 mM tetra-*n*-butylammonium hexafluorophosphate. For Ga-1, 2% pyridine was added to maintain the axial ligand.

a 300 mV shift between gallium and phosphorus corrole analogues, and an additional 340 mV shift to higher potentials by chlorinating the eight β ring positions. Using the potential for oxidation and excited-state energies, the excited-state reduction potentials were calculated and shown in Table 1 along with a summary of the photophysical properties of the corroles.

Table 1. Corrole Physical, Photophysical, and Electrochemical Properties

dye	absorbance[a]	E_{0-0}[a,c]	τ_{fl}[a,c]	E_{ox1}[b,c]	E_{ox}*[d]
	λ_{max}/nm (ε x 10^{-4} M^{-1} cm^{-1})	eV	ns	V vs NHE	
Ga-1	430 (24.2), 534 (1.00), 572 (1.41), 614 (4.10)	2.00	2.3	0.78	−1.22
P-1	417 (27.2), 524 (1.05), 562 (1.43), 597 (4.31)	2.06	3.0	1.08	−0.98
PCl_8-1	401 (5.40), 424 (28.3), 534 (1.05), 557 (1.13), 600 (3.27)	2.05	0.66	1.42	−0.63

[a]Values for Ga-1, P-1, and PCl_8-1 obtained in dichloromethane solvent. [b]Values for $E_{1/2}$. Electrochemistry performed in dichloromethane containing 100 mM $TBAPF_6$ electrolyte with ferrocene as internal reference. Oxidations were reversible. [c]Solvent contained 2% pyridine when examining Ga-1. [d]The excited-state reduction potentials, E_{ox}*, were calculated as $E_{ox1} - E_{0-0}$.

Spectroelectrochemistry of the corroles in dichloromethane solution was performed to determine the UV−visible absorbance spectra of the corrole radical cation species. Upon oxidation, the spectral changes observed in Figure 4 reveal a decrease in absorbance around the Q-band region and a new broadly absorbing peak extending into the NIR region. These spectroscopic features guide the choice of optimal wavelengths to monitor formation of the corrole radical cation using transient absorption spectroscopy of the dye-sensitized metal oxide films.

For anchoring to TiO_2 surfaces, the monocarboxylic acid corrole analogues Ga-2, P-2, and PCl_8-2 were prepared by alkaline hydrolysis of the diester analogues. DSSCs were prepared using the iodide-triiodide redox couple as a model system to compare dye properties and performance. The electrolyte consisted of 100 mM LiI, 50 mM I_2, 100 mM *tert*-butylpyridine (TBP), and 800 mM *n*-butylmethylimidazolium iodide in acetonitrile solvent. The incident photon to current efficiency (IPCE) spectra in Figure 5 show modest values with features similar to the dye UV−visible absorbance spectra. At wavelengths around the Soret where all photons are absorbed, the nonchlorinated phosphorus corrole P-2 had the highest conversion efficiencies followed by Ga-2. The chlorinated phosphorus corrole PCl_8-2 had negligible values where the corrole absorbed. Under AM1.5G simulated sunlight at 1000 W/m^2 intensity, the photoelectrochemical cells had J_{sc} values that were consistent with the IPCE data (Figures 5 and 6). DSSC analyses are summarized for each dye in Table 2. P-2 showed the highest solar conversion efficiency of 1.9%, with Ga-2 at 0.73% and PCl_8-2 at 0.02%. For Ga-2 and P-2, fill factors were comparable (~0.60) with slightly higher V_{oc} for P-2 (507 vs 471 mV).

The low efficiency of the DSSC incorporating PCl_8-2 may be due to E_{ox}* for this molecule being too positive for efficient electron injection into the TiO_2 conduction band (Table 1). The role of photoinduced electron injection efficiency was probed for PCl_8-2 by altering the electrolyte to make the TiO_2 conduction band more accessible to the photoexcited dye. This electrolyte contained 500 mM LiI, 50 mM I_2, and 10 mM TBP in acetonitrile solvent. The increased $[Li^+]$ and decreased [TBP] shifts the conduction band to more positive potentials.[1] The DSSC J_{sc} increased to 2.48 mA/cm^2, with a V_{oc} of 392 mV, fill factor of 0.60, and overall efficiency of 0.58% (Figure S3 of the Supporting Information). This increase provides evidence that electron injection was limiting the system performance.

To analyze more fully the role of dye properties on the photoelectrochemical cell performance, the photosensitized TiO_2 films were examined by transient absorption spectroscopy (TA). After laser excitation and photoinduced electron injection, the corrole radical cation species oxidizes iodide in competition with electron−hole recombination with the injected electron. These processes can be followed by TA using the spectroscopic handles determined from spectroelectrochemistry of the corroles in solution (Figure 4). When the dye-sensitized TiO_2 films were immersed in inert electrolyte consisting of 100 mM $LiClO_4$ and 100 mM TBP in acetonitrile, laser photoexcitation of the corroles in the Q-band region led to the formation of a species with NIR absorbance consistent with that of the corrole radical cation (Figure S4 of the Supporting Information). This species decays (Figure 7) on the microsecond time scale by electron−hole recombination, and could be fit by a stretched-exponential function based on the Kohlrausch−Williams−Watts (KWW) model shown in eq

DOI: 10.1021/acsami.5b05050
ACS Appl. Mater. Interfaces 2015, 7, 16124−16130

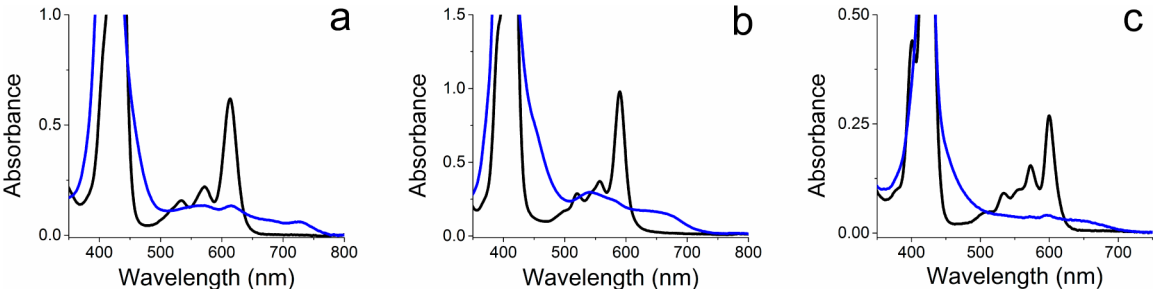

Figure 4. Spectroelectrochemistry of corroles. Spectra determined for (a) Ga-1, (b) P-1, and (c) PCl_8-1 in CH_2Cl_2 containing 100 mM tetra-*n*-butylammonium hexafluorophosphate, before (black) and after (blue) bulk electrolysis of the solution to form the oxidized corrole radical cation. For Ga-1, 2% pyridine added to maintain the axial ligand.

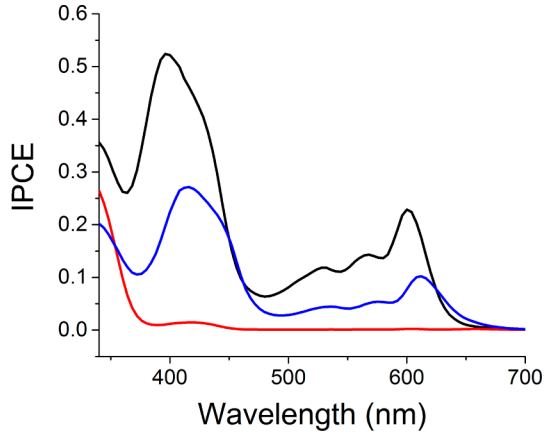

Figure 5. Corrole IPCE spectra for Ga-2 (blue), P-2 (black), and PCl_8-2 (red). Electrolyte consisted of 100 mM LiI, 50 mM I_2, 100 mM *tert*-butylpyridine, and 800 mM *n*-butylmethylimidazolium iodide in acetonitrile solvent.

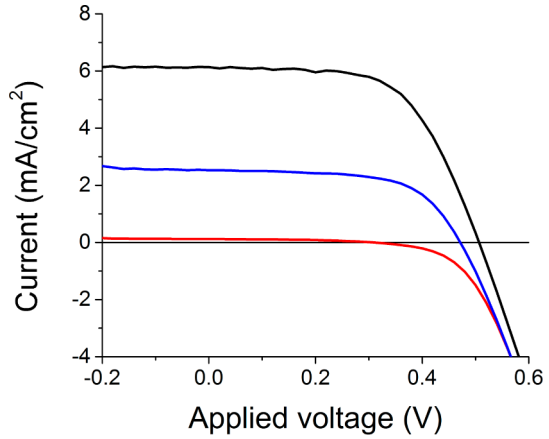

Figure 6. *I*–*V* data under 1000 W/m^2 illumination for Ga-2 (blue), P-2 (black), and PCl_8-2 (red) using electrolyte consisting of 100 mM LiI, 50 mM I_2, 100 mM *tert*-butylpyridine, and 800 mM *n*-butylmethylimidazolium iodide in acetonitrile solvent.

1.[16−18] The transient absorption signal (ΔOD) is related to the rate of recombination k_{rec}, and the KWW model incorporates the heterogeneity of the system with a distribution of rate constants using β with values between 0 and 1. *A*, *t*, and t_0 are initial intensity, time, and initial time, respectively. The recombination lifetime τ_{TWW} can be determined using eq 2, where the Γ-function is employed as previously discussed by Meyer et al.[18] Values of τ_{TWW} and (β) were determined to be

Table 2. DSSC Analysis[a]

	J_{sc} (mA/cm^2)	V_{oc} (mV)	FF	η (%)
Ga-2	2.53	471	0.62	0.73
P-2	6.36	507	0.58	1.9
PCl_8-2	0.25	306	0.21	0.02

[a]DSSCs prepared using TiO_2 films on FTO glass with platinized FTO counter electrode. Electrolyte consisted of 100 mM LiI, 50 mM I_2, 100 mM *tert*-butylpyridine, and 800 mM *n*-butylmethylimidazolium iodide in acetonitrile solvent. Data obtained using AM1.5G 1000 W/m^2 simulated sunlight.

87 μs (0.46), 80 μs (0.45), and 11 μs (0.47) for Ga-2, P-2, and PCl_8-2, respectively.

$$\Delta OD = Ae^{-[k_{rec}(t-t_0)]^{\beta}} \quad (1)$$

$$\tau_{TWW} = \frac{\Gamma(\beta^{-1})}{k_{rec}\beta} \quad (2)$$

The rate of iodide quenching by the corrole radical cation was determined from TA kinetic traces shown in Figure 7, and the quenching percentages were obtained by comparing the time-resolved decay of the corrole radical cation on photosensitized TiO_2 electrodes immersed in inert solvent and in the DSSC solvent containing iodide. The data were fit to eq 3, simulating the competitive recombination and quenching processes. Here, A_1 and A_2 are the relative contributions of each process to the overall decay, with the quenching efficiency estimated as $A_2/(A_1 + A_2)$. It is important to note that β, a variable generally attributed to the broad distribution of recombination rate constants in the heterogeneous surface environment, was found to be relatively consistent for both recombination and quenching processes, and so was held as a constant. This was especially evident in the case of Ga-2, where there are similar contributions from both processes. We postulate that diffusion of iodide in the randomly porous network causes similar distributions of regeneration kinetics as those of the recombination kinetics on the heterogeneous surface.

$$\Delta OD = A_1e^{-[k_{rec}(t-t_0)]^{\beta}} + A_2e^{-[k_{quench}(t-t_0)]^{\beta}} \quad (3)$$

From Figure 7, the corrole radical cation lifetime is substantially decreased in the presence of iodide, which reduces the cation back to its ground state. However, the rate of quenching was substantially different with each dye. Without iodide, the corrole radical cation decayed on the microsecond time scale. With iodide, the oxidized dye has a competitive electrochemical reaction to oxidize iodide, with the rate

DOI: 10.1021/acsami.5b05050
ACS Appl. Mater. Interfaces 2015, 7, 16124−16130

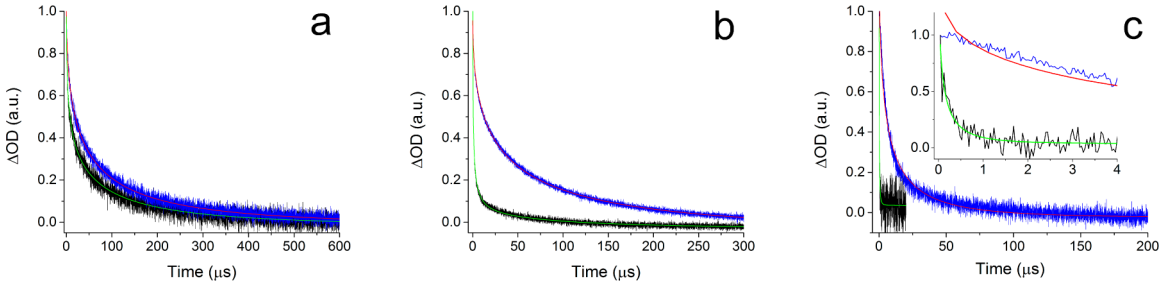

Figure 7. Transient absorbance kinetic decays in inert electrolyte (blue) and redox-active electrolyte (black) with fits overlaid for (a) Ga-2, (b) P-2, and (c) PCl_8-2 on TiO_2. The inset highlights the earlier time periods for the PCl_8-2 data. Dye-sensitized electrodes were photoexcited at 615 nm for Ga-2, and 600 nm for P-2 and PCl_8-2, with kinetic traces obtained at 740 nm for Ga-2 and 650 nm for P-2 and PCl_8-2. Inert electrolyte consisted of 100 mM $LiClO_4$ and 100 mM *tert*-butylpyridine in acetonitrile. Redox-active iodide-containing electrolyte consisted of 100 mM LiI, 50 mM I_2, 100 mM *tert*-butylpyridine, and 800 mM *n*-butylmethylimidazolium iodide in acetonitrile solvent.

dependent on the driving force for the reaction. Quenching efficiencies of 30%, 83%, and 99.5% were determined for Ga-2, P-2, and PCl_8-2, respectively, with additional information provided in Table S1 of the Supporting Information. The radical cation of Ga-2 is the least oxidizing at 0.78 V vs NHE, and has the slowest rate for oxidizing iodide ($k_{ox} = 8.4 \times 10^5$ s^{-1} M^{-1}, where $k_{ox} = k_{quench}/[I^-]$). The radical cation of PCl_8-2 is the most powerful oxidant at 1.42 V and has the fastest quenching rate ($k_{ox} = 1.8 \times 10^7$ s^{-1} M^{-1}). P-2 has an electrochemical potential for oxidation and a quenching rate between the two ($k_{ox} = 1.9 \times 10^6$ s^{-1} M^{-1}).

DISCUSSION

In this study, we have obtained structure−function information on the performance of corroles as photosensitizers in photoelectrochemical cells. These results have yielded new data on the photophysical properties of corroles and their applicability in photoelectrochemical cells. Corroles have significant structural flexibility for tuning electrochemical potentials while maintaining the photophysical properties required for photoinduced electron-transfer processes. From the same basic macrocycle ligand, the 300 mV difference in electrochemical potentials for oxidation of Ga-1 and P-1, and an additional 340 mV between P-1 and PCl_8-1, reveals a wide window for electrochemical tuning. The more electron deficient P(V) compared to Ga(III) is the cause of the difference between the chelated corroles, whereas *β*-chlorination further removes electron density from the ring via inductive effects. The observed 640 mV window could also be extended by varying the *meso*-aryl substituents. In addition, changing the chelated species from gallium to phosphorus did not significantly degrade the important photophysical properties of the singlet excited state required for efficient function of a dye as a photosensitizer in a photoelectrochemical cell. *β*-octachlorination of P-1 to PCl_8-1 decreased the singlet excited-state lifetime by ∼5 fold, whereas porphyrins have been shown to have a similar decrease after only *β*-dichlorination.[19] These decreases have been shown to originate from heavy atom effects increasing the rate of triplet conversion.[19,20] Corroles generally have higher quantum yields of fluorescence compared to porphyrins, and might be buffering the system from a substantial quenching of the fluorescence.[15] With PCl_8-1 still maintaining a 660 ps singlet state lifetime, similar to other organic dyes such as MK-2 that are used in highly efficient DSSCs, its photophysical properties are suitable for photoinduced electron-transfer processes.[21] Thus, with the flexibility of corroles appearing to surpass that of porphyrins, molecular engineering of corroles is possible to tune properties for photoelectrochemical applications. Specifically, P-1 and PCl_8-1 derivatives have potentials for oxidation that enable them to be thermodynamically capable of the water-oxidation reaction in a wide pH range, suggesting they could be utilized alongside a catalyst in photoelectrochemical water-oxidation cell designs.

When integrated into model DSSCs, the molecules showed significant differences in efficiencies. Although the general light harvesting features (Figure 2) and singlet energies (E_{0-0}/Table 1) among Ga-1, P-1, and PCl_8-1 are similar, the differences in electrochemical properties (Figure 3) had a profound effect on DSSC performance. The IPCE spectra and *I*−*V* data in Figures 5 and 6 show that use of P-2 (η = 1.9%) results in the most efficient DSSC of the three corroles. The internal quantum efficiency (# electrons/absorbed photon) can be approximated as the IPCE value near the highly absorbing Soret wavelength where all photons are absorbed, with P-2 having a peak value of 0.52. This is similar to analogously simple Zn-porphyrins,[22] providing evidence that corroles have potential as photosensitizers in photoelectrochemical cells.

Both Ga-2 and PCl_8-2 produced significantly less efficient DSSCs than P-2, the origin of which was explored further. From the photophysical and electrochemical data provided in Table 1, it was hypothesized that the radical cation of Ga-2 might have difficulty oxidizing the redox couple in competition with recombination. The potential for oxidation of the model compound Ga-1 was 0.78 V vs NHE, whereas the $I_2^{\cdot-}/I^-$ redox process that has been associated with regeneration has been estimated to be <0.93 V vs NHE.[23,24] Both P-1 and PCl_8-1 have potentials for oxidation above this value. TA spectroscopy of the dye-sensitized electrodes in inert electrolyte or containing iodide (Figure 7) confirm that Ga-2 was only 30% regenerated by iodide, with detrimental recombination significantly decreasing the efficiency of the photoelectrochemical cell. The greater driving force for regeneration by P-2 and PCl_8-2 radical cations allowed for much higher rates of iodide oxidation, decreasing the competitiveness of recombination between the dye hole and semiconductor electron.

PCl_8-2, although having very fast regeneration kinetics, was hypothesized to have inefficient photodriven electron injection into the TiO_2 conduction band. The calculated excited-state electrochemical potential of the model compound PCl_8-1 (−0.63 V vs NHE) was found to be more positive than the commonly referenced TiO_2 conduction band potential of −0.66 V vs NHE, suggesting that injection would be a thermodynamically uphill process.[25] The negligible solar conversion efficiency from PCl_8-2 supported this conclusion.

DOI: 10.1021/acsami.5b05050
ACS Appl. Mater. Interfaces 2015, 7, 16124−16130

However, the TiO_2 conduction band electrochemical potential varies with the electrolyte composition. Electrolyte additives can significantly shift this potential, with Li^+ making the value more positive and TBP more negative.[1] DSSCs using PCl_8-2 were compared using two electrolytes containing different concentrations of the Li^+ and TBP additives. When [Li^+] was increased from 100 to 500 mM, and [TBP] decreased from 100 to 10 mM, the conduction band shifted to more positive values and became more thermodynamically accessible for the photoexcited PCl_8-2. Values for J_{sc} rose 10-fold from 0.25 to 2.48 mA/cm^2 (Figure S3 of the Supporting Information), increasing the solar conversion efficiency from 0.02% to 0.58% and providing evidence that electron injection was the limiting factor. The relatively low V_{oc} of 392 mV obtained using the altered electrolyte, compared to Ga-2 and P-2 photoelectrochemical cells (471−507 mV), suggests that alteration of the electrolyte shifted the conduction band potential by ∼100 mV.

CONCLUSIONS

Corrole molecular designs for solar applications are currently at a stage where porphyrin dyes were nearly 2 decades ago, with many structure−function relationships not yet explored in detail. Here, three dyes (Ga, P, PCl_8) were examined for their physical, photophysical, electrochemical, and photoelectrochemical properties. Analyses revealed that corroles have similar photophysical and spectroelectrochemical properties to porphyrins, with significant flexibility in their electrochemical properties. As photoelectrochemical cells are based on a cascade of electron transfers, tuning the electrochemical potentials allows for optimizing the thermodynamic and kinetic properties to achieve the most efficient photoelectrochemical cell. We determined that after photoinduced electron injection, the Ga-2 corrole radical cation underwent slow regeneration with iodide due to a low driving force for the electrochemical reaction. We also determined that PCl_8-2 was limited by its efficiency of electron injection into TiO_2 due to a lack of driving force from the photoexcited state. Injection efficiency was increased by adjusting the TiO_2 conduction band electrochemical potential with an electrolyte containing greater [Li^+] and lower [TBP]. The corrole with the highest efficiency, P-2, was determined to have thermodynamic driving force for both photoinduced electron injection and subsequent oxidation of iodide by the corrole radical cation. Thus, the electrochemical properties for corroles are highly tunable, and care must be taken to design dyes with suitable electrochemical potentials for the redox processes involved in the particular photoelectrochemical cell. These results provide structure−function data for tuning these electrochemical potentials and a route to design more complex corroles for a wide variety of photoelectrochemical systems. Furthermore, our results show that phosphorus corroles with β-chlorination afford dyes with significant anodic shifts in electrochemical potentials−substantially higher than that of water oxidation for a wide pH range−while still maintaining singlet excited-state lifetimes amenable to photoinduced charge transfer processes. The chlorinated macrocycle should also be more chemically stable under oxidative conditions than its nonchlorinated analogue. These attributes make PCl_8-2 an attractive molecule for further tuning with the ultimate goal of developing a photodriven water-oxidation photoelectrochemical cell.

ASSOCIATED CONTENT

Supporting Information

Experimental methods for corrole syntheses, corrole fluorescence and transient absorption spectra, iodide oxidation kinetic parameters, and additional IPCE and $I-V$ spectra for PCl_8-2. The Supporting Information is available free of charge on the ACS Publications website at DOI: 10.1021/acsami.5b05050.

AUTHOR INFORMATION

Corresponding Author

*G. W. Brudvig. E-mail: gary.brudvig@yale.edu.

Notes

The authors declare no competing financial interest.

ACKNOWLEDGMENTS

This work was supported by a generous donation from the TomKat Charitable Trust. Additional support from the U.S. Department of Energy, Chemical Sciences, Geosciences, and Biosciences Division, Office of Basic Energy Sciences, Office of Science (DE-FG02-07ER15909) is gratefully acknowledged.

REFERENCES

(1) Hagfeldt, A.; Boschloo, G.; Sun, L.; Kloo, L.; Pettersson, H. Dye-Sensitized Solar Cells. *Chem. Rev.* **2010**, *110* (11), 6595−6663.

(2) Hambourger, M.; Brune, A.; Gust, D.; Moore Ana, L.; Moore Thomas, A. Enzyme-assisted Reforming of Glucose to Hydrogen in a Photoelectrochemical Cell. *Photochem. Photobiol.* **2005**, *81* (4), 1015−20.

(3) Moore, G. F.; Blakemore, J. D.; Milot, R. L.; Hull, J. F.; Song, H.; Cai, L.; Schmuttenmaer, C. A.; Crabtree, R. H.; Brudvig, G. W. A Visible Light Water-splitting Cell with a Photoanode Formed by Codeposition of a High-potential Porphyrin and an Iridium Water-oxidation Catalyst. *Energy Environ. Sci.* **2011**, *4* (7), 2389.

(4) Li, L. L.; Diau, E. W. G. Porphyrin-sensitized Solar Cells. *Chem. Soc. Rev.* **2013**, *42* (1), 291.

(5) Swierk, J. R.; Méndez-Hernández, D. D.; McCool, N. S.; Liddell, P.; Terazono, Y.; Pahk, I.; Tomlin, J. J.; Oster, N. V.; Moore, T. A.; Moore, A. L.; Gust, D.; Mallouk, T. E. Metal-free Organic Sensitizers for Use in Water-splitting Dye-sensitized Photoelectrochemical Cells. *Proc. Natl. Acad. Sci. U. S. A.* **2015**, *112* (6), 1681−1686.

(6) Sudhakar, K.; Giribabu, L.; Salvatori, P.; Angelis, F. D. Triphenylamine-functionalized Corrole Sensitizers for Solar-cell Applications. *Phys. Status Solidi A* **2015**, *212* (1), 194−202.

(7) Walker, D.; Chappel, S.; Mahammed, A.; Brunschwig, B. S.; Winkler, J. R.; Gray, H. B.; Zaban, A.; Gross, Z. Corrole-sensitized TiO_2 solar cells. *J. Porphyrins Phthalocyanines* **2006**, *10* (11), 1259−1262.

(8) Brennan, B. J.; Keirstead, A. E.; Liddell, P. A.; Vail, S. A.; Moore, T. A.; Moore, A. L.; Gust, D. 1-(3′-Amino)propylsilatrane Derivatives as Covalent Surface Linkers to Nanoparticulate Metal Oxide Films for Use in Photoelectrochemical Cells. *Nanotechnology* **2009**, *20* (50), 505203.

(9) Laha, J. K.; Dhanalekshmi, S.; Taniguchi, M.; Ambroise, A.; Lindsey, J. S. A Scalable Synthesis of Meso-Substituted Dipyrromethanes. *Org. Process Res. Dev.* **2003**, *7* (6), 799−812.

(10) Koszarna, B.; Gryko, D. T. Efficient Synthesis of meso-Substituted Corroles in a H_2O−MeOH Mixture. *J. Org. Chem.* **2006**, *71* (10), 3707−3717.

(11) Noviandri, I.; Brown, K. N.; Fleming, D. S.; Gulyas, P. T.; Lay, P. A.; Masters, A. F.; Phillips, L. The Decamethylferrocenium/Decamethylferrocene Redox Couple: A Superior Redox Standard to the Ferrocenium/Ferrocene Redox Couple for Studying Solvent Effects on the Thermodynamics of Electron Transfer. *J. Phys. Chem. B* **1999**, *103* (32), 6713−6722.

(12) Barea, E. M.; Gónzalez-Pedro, V.; Ripollés-Sanchis, T.; Wu, H. P.; Li, L. L.; Yeh, C. Y.; Diau, E. W. G.; Bisquert, J. Porphyrin Dyes

DOI: 10.1021/acsami.5b05050
ACS Appl. Mater. Interfaces 2015, 7, 16124−16130

with High Injection and Low Recombination for Highly Efficient Mesoscopic Dye-Sensitized Solar Cells. *J. Phys. Chem. C* **2011**, *115* (21), 10898−10902.
(13) Bendix, J.; Dmochowski, I. J.; Gray, H. B.; Mahammed, A.; Simkhovich, L.; Gross, Z. Structural, Electrochemical, and Photophysical Properties of Gallium(III) 5,10,15-Tris(pentafluorophenyl)-corrole. *Angew. Chem., Int. Ed.* **2000**, *39* (22), 4048−4051.
(14) Ghosh, A.; Ravikanth, M. Synthesis, Structure, Spectroscopic, and Electrochemical Properties of Highly Fluorescent Phosphorus(V)-meso-Triarylcorroles. *Chem. - Eur. J.* **2012**, *18* (20), 6386−6396.
(15) Aviv-Harel, I.; Gross, Z. Coordination Chemistry of Corroles with Focus on Main Group Elements. *Coord. Chem. Rev.* **2011**, *255* (7−8), 717−736.
(16) Williams, G.; Watts, D. C. Non-symmetrical Dielectric Relaxation Behaviour Arising from a Simple Empirical Decay Function. *Trans. Faraday Soc.* **1970**, *66* (0), 80−85.
(17) Lindsey, C. P.; Patterson, G. D. Detailed Comparison of the Williams−Watts and Cole−Davidson Functions. *J. Chem. Phys.* **1980**, *73* (7), 3348.
(18) Abrahamsson, M.; Johansson, P. G.; Ardo, S.; Kopecky, A.; Galoppini, E.; Meyer, G. J. Decreased Interfacial Charge Recombination Rate Constants with N3-Type Sensitizers. *J. Phys. Chem. Lett.* **2010**, *1* (11), 1725−1728.
(19) Bonnett, R.; Harriman, A.; Kozyrev, A. N. Photophysics of Halogenated Porphyrins. *J. Chem. Soc., Faraday Trans.* **1992**, *88* (6), 763−769.
(20) Nardis, S.; Mandoj, F.; Paolesse, R.; Fronczek, F. R.; Smith, K. M.; Prodi, L.; Montalti, M.; Battistini, G. Synthesis and Functionalization of Germanium Triphenylcorrolate: The First Example of a Partially Brominated Corrole. *Eur. J. Inorg. Chem.* **2007**, *2007* (16), 2345−2352.
(21) Koenigsmann, C.; Ripolles, T. S.; Brennan, B. J.; Negre, C. F. A.; Koepf, M.; Durrell, A. C.; Milot, R. L.; Torre, J. A.; Crabtree, R. H.; Batista, V. S.; Brudvig, G. W.; Bisquert, J.; Schmuttenmaer, C. A. Substitution of a Hydroxamic Acid Anchor into the MK-2 Dye for Enhanced Photovoltaic Performance and Water Stability in a DSSC. *Phys. Chem. Chem. Phys.* **2014**, *16* (31), 16629−16641.
(22) Imahori, H.; Hayashi, S.; Hayashi, H.; Oguro, A.; Eu, S.; Umeyama, T.; Matano, Y. Effects of Porphyrin Substituents and Adsorption Conditions on Photovoltaic Properties of Porphyrin-Sensitized TiO_2 Cells. *J. Phys. Chem. C* **2009**, *113*, 18406−18413.
(23) Boschloo, G.; Hagfeldt, A. Characteristics of the Iodide/Triiodide Redox Mediator in Dye-Sensitized Solar Cells. *Acc. Chem. Res.* **2009**, *42*, 1819−1826.
(24) Wang, X.; Stanbury, D. M. Oxidation of Iodide by a Series of Fe(III) Complexes in Acetonitrile. *Inorg. Chem.* **2006**, *45* (8), 3415−3423.
(25) Redmond, G.; Fitzmaurice, D. Spectroscopic Determination of Flatband Potentials for Polycrystalline Titania Electrodes in Non-aqueous Solvents. *J. Phys. Chem.* **1993**, *97* (7), 1426−1430.

DOI: 10.1021/acsami.5b05050
ACS Appl. Mater. Interfaces 2015, 7, 16124−16130